Effects of relaxation and Auger decay on photoionization calculations of argon

M. Kutzner,[1] Q. Shamblin,[1] S. E. Vance,[2] and D. Winn[3]
[1]*Physics Department, Andrews University, Berrien Springs, Michigan 49104*
[2]*Department of Physics, Columbia University, New York, New York 10027*
[3]*Department of Physics, University of Michigan, Ann Arbor, Michigan 48109-1120*
(Received 2 January 1996)

Photoionization cross sections, branching ratios, and photoelectron angular-distribution asymmetry parameters have been calculated for all Ar ($Z=18$) subshells using the relativistic random-phase approximation, the relativistic random-phase approximation modified to include relaxation effects, and the relativistic random-phase approximation modified to include relaxation effects and Auger decay. Comparisons are made between the various theoretical results and experimental data. The importance of relaxation and Auger decay is seen to increase for deep inner subshells, particularly $1s$ and $2s$. [S1050-2947(96)00612-9]

PACS number(s): 32.80.Hd, 32.80.Fb

I. INTRODUCTION

The argon atom ($Z=18$) has been the subject of many photoionization studies by both experimentalists and theorists. The closed-shell structure makes an analysis of argon accessible to a large variety of theoretical techniques. Each subshell, from the valence $3p$ down to the innermost $1s$, offers new challenges to theory for unique reasons.

The photoionization cross section near the valence threshold was measured nearly three decades ago by Samson [1]. Since then, Marr and West [2] and Chang [3] have also measured the total photoionization cross section in this region. Houlgate *et al.* [4] measured the photoelectron angular-distribution asymmetry parameter for $3p$ electrons. Many theoretical models of photoionization including the many-body perturbation theory (MBPT) [5], the random-phase approximation with exchange (RPAE) [6], and the relativistic random-phase approximation [7] were tested early on the $3p$ subshell of argon. All have demonstrated the importance of including intrachannel interactions and random-phase approximation contributions in the theories.

Photoionization from the $3s$ subshell has attracted a great deal of attention recently. The overall shape of the cross section is driven strongly by interchannel coupling with the $3p$ subshell [8]. Strong satellite lines in the photoelectron spectra [9] have been observed indicating the presence of photoionization-with-excitation channels. Very recent measurements of Möbus *et al.* [10] using photon-induced fluorescence spectroscopy and time-of-flight photoelectron spectroscopy have greatly enhanced the accuracy of cross sections and photoelectron angular-distribution asymmetry parameters in this region.

Experimental measurements of the $2p$ subshell photoionization cross section were carried out in the 1960s [11–13]. Lindle *et al.* [14] and Avaldi *et al.* [15] have measured the photoelectron angular-distribution asymmetry parameter for $2p$ electrons. Amusia and Cherepkov [6] used the generalized relativistic random-phase approximation (GRPAE) to demonstrate the importance of relaxation in this region.

The $2s$ subshell of argon has had the least attention from both the experimental and theoretical perspectives. Lukirskii and Zimkina [16] measured the photoionization cross section above the $2s$ threshold with low accuracy. Lavrentev *et al.* [17] showed theoretically the effects of relaxation above the $2s$ threshold using many-body perturbation theory in the framework of the RPAE.

The near-threshold K-shell photoabsorption cross section of argon has become a showcase of correlation phenomena. A comparison of the experimental work of Deslattes *et al.* [18] with a number of theoretical calculations has demonstrated the need for inclusion of such many-body effects as core relaxation [19,20], Auger decay [21], and configuration interaction [22].

The present work is a subshell-by-subshell theoretical investigation of the photoionization of argon atoms to determine the effects of core relaxation and (where appropriate) Auger decay on cross sections, branching ratios, and photoelectron angular-distribution parameters. We have attempted in the case of each subshell to make comparisons between the latest experimental results and three theoretical models, namely, the relativistic random-phase approximation (RRPA), the relativistic random-phase approximation modified to include relaxation effects (RRPAR), and the newly developed relativistic random-phase approximation modified to include relaxation and Auger decay (RRPARA). Comparisons presented in this way give valuable insights into the effects of various types of electron correlation.

II. METHOD

Detailed discussions of both the RRPA and the RRPAR can be found elsewhere [23,24]. Here we will point out that in the RRPA, the partial photoionization cross section for a given subshell is given by

$$\sigma_{n\kappa}=\frac{4\pi^2\alpha\omega}{3}(|D_{nj\rightarrow j-1}|^2+|D_{nj\rightarrow j}|^2+|D_{nj\rightarrow j+1}|^2). \quad (1)$$

In this equation, n is the principal quantum number and $\kappa=\mp(j+1/2)$ for $j=l\pm1/2$, where j and l are the single-electron total and orbital angular-momentum quantum numbers. The dipole matrix element $D_{nj\rightarrow j'}$ is the reduced RRPA dipole matrix element for the photoionization channel $nj\rightarrow j'$.

The angular-distribution asymmetry parameter $\beta_{n\kappa}$ for the subshell $n\kappa$ is defined in terms of the differential cross section as

$$\frac{d\sigma_{n\kappa}}{d\Omega}=\frac{\sigma_{n\kappa}(\omega)}{4\pi}\left[1-\frac{1}{2}\beta_{n\kappa}(\omega)P_2(\cos\theta)\right], \tag{2}$$

where ω is the photon energy and θ is the angle measured between the direction of the incident photon and the photoelectron. When a subshell is split by spin-orbit splitting into two different levels $j=l\pm 1/2$, it is conventional to use the weighted average given by

$$\beta_{nl}=\frac{\sum_{\kappa=-(l+1),l\kappa\neq 0}\beta_{n\kappa}\sigma_{n\kappa}}{\sum_{\kappa=-(l+1),l\kappa\neq 0}\sigma_{n\kappa}}. \tag{3}$$

The RRPAR method approximates the effects of core relaxation by calculating the continuum photoelectron orbital in the potential of the relaxed ion. The ionic core with the hole in the level with $j=l+1/2$ has a lower ionization threshold energy and also represents the most populated of the two levels. Thus we generally place the hole in the subshell with the largest j for the purpose of obtaining the V^{N-1} potential. Overlap integrals of the form $\mathrm{Det}\langle\phi_i'|\phi_i\rangle$ between orbitals of the unrelaxed ground state ϕ_i and the corresponding orbitals of the final relaxed state ϕ_i' are included in the RRPAR dipole matrix element for each electron i of the ionic core. Inclusion of these overlap integrals is important for calculation of the partial photoionization cross sections since they approximately remove oscillator strength due to double-excitation shake-up and shake-off processes from the single-excitation channel oscillator strength [25]. To approximately include the effects of Auger decay, we add to the RRPAR dipole matrix element contributions involving overlap integrals between orbitals of the ground state and the continuum orbitals of the final state. According to Åberg [26], this factorization of the post-collision interaction matrix element into a one-electron energy-dependent Auger decay amplitude and the one-electron overlap matrix element is equivalent to approximating that the many-electron Hamiltonian matrix element that involves the final scattering wave function describes the emission of the slow photoelectron and the fast Auger electron.

Photoionization thresholds in the strict RRPA model are the Dirac-Hartree-Fock (DHF) eigenvalues. However, experimental thresholds are frequently utilized. In this work we have used DHF threshold energies for RRPA caculations. In the RRPAR and RRPARA, we have used the experimental ionization energies for calculations involving relaxation of holes in the various subshells. The DHF energies we used were obtained using the Oxford multiconfiguration Dirac-Fock computer code of Grant *et al.* [27] and the experimental values used were from Ref. [28]. Table I summarizes the DHF and experimental energies used for all the channels incorporated in the present study. Note that subshells where the experimental threshold closely matches the difference in total self-consistent field energies of the neutral atom and ion (ΔE_{SCF}) are also subshells where relaxation effects are found to be important.

TABLE I. Photoionization thresholds (in a.u.) for the various subshells of atomic argon. The second column lists the absolute values of single-particle eigenvalues from a Dirac-Hartree-Fock (DHF) calculation. The third column lists experimental thresholds from Siegbahn and Karlsson [28]. The fourth column lists the absolute value of the difference between self-consistent field calculations of total energy of the neutral atom and the ion (ΔE_{SCF}).

Subshell J	DHF	Experiment	ΔE_{SCF}
$1s_{1/2}$	119.12688	117.814	117.934936
$2s_{1/2}$	12.411606	11.994	12.0249023
$2p_{1/2}$	9.6319574	9.215560	9.20477195
$2p_{3/2}$	9.5470662	9.136652	9.12316894
$3s_{1/2}$	1.2865872	1.0767	1.22851563
$3p_{1/2}$	0.59538510	0.58567	0.54669189
$3p_{3/2}$	0.58782064	0.57916	0.53991699

The RRPA theory predicts results that are gauge independent provided that one has included all possible dipole-excited channels [23]. In practice, where one limits the number of channels (the truncated RRPA), there will be differences between the ''length'' and ''velocity'' gauge results. Also, the inclusion of relaxation effects in the RRPAR and RRPARA potentials leads to differences in calculations performed in the two gauges. In the present calculations, we included all 16 dipole allowed channels. Hence results of calculations performed in the RRPA have the geometric mean of the length and velocity results shown in the figures; RRPAR results often have both length and velocity results plotted individually. Discrepancies between length and velocity results for the RRPARA are similar to those for RRPAR.

III. RESULTS

A. The 3*p* subshell

Photoionization in the vicinity of the valence-shell threshold of argon atoms has been the focus of many experimental [1–4] and theoretical [5–7] studies. In particular, experimental measurements of the total photoionization cross section have been reported by a number of workers [1–3]. Theoretical investigations employing the RPAE [6], RRPA [7], and MBPT [5,29] have all been used to study this region. Tulkki and Åberg [19] calculated the effects of relaxation on the $3p$ subshell cross section using the multiconfiguration multichannel Dirac-Fock (MMCDF) method and found the differences between relaxed and unrelaxed calculations to be modest. Large relaxation effects are not expected for valence photoionization since by Gauss's law the potentials for inner-shell electrons are affected little by the presence or absence of a valence electron.

Total photoionization cross section results for the present work are shown in Fig. 1(a) along with the experiments of Samson [1], Marr and West [2], and Chang [3]. When displaying the RRPA results, we show only the geometric mean of length and velocity calculations since the two agree well; the RRPAR length and velocity results are shown separately

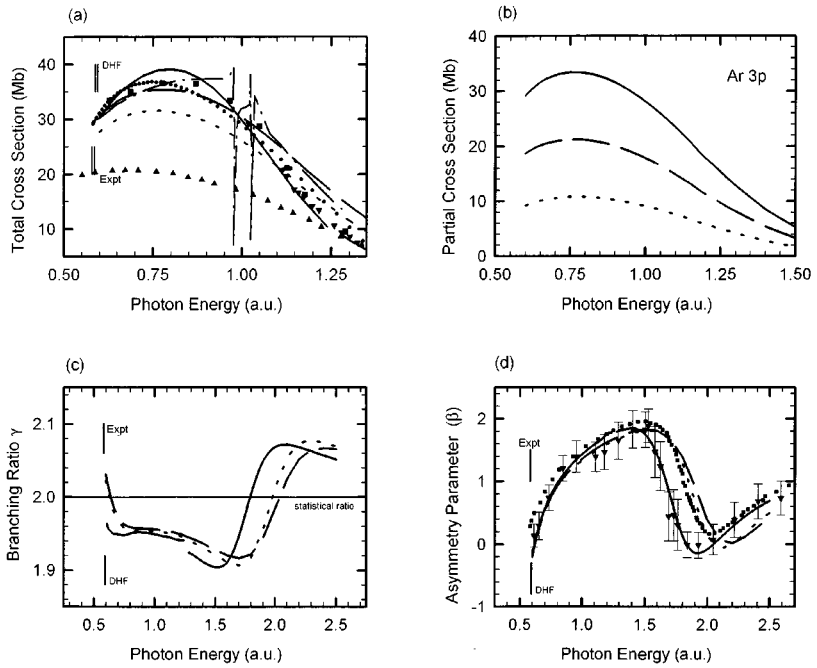

FIG. 1. Photoionization parameters for the $3p$ subshells of atomic argon. Solid curves represent RRPA results and dashed (dotted) lines are the RRPAR length (velocity) results of this work. (a) Total photoionization cross section where experimental data are represented by solid dots, Marr and West [2]; inverted triangles, Samson [1]; and solid squares, Chang [3]. MMCDF calculations [30] are represented by triangles and MBPT [29] by the dashed curve. (b) Partitioning of the total absorption cross section into partial cross sections. The solid line is the total, the dashed line is the $3p_{3/2}$, and dotted line is the $3p_{1/2}$ cross section. (c) Branching ratios $\gamma=\sigma(3p_{3/2})/\sigma(3p_{1/2})$ with the same lines as in (a). (d) Photoelectron angular-distribution asymmetry parameters with the experimental data from Houlgate *et al.* [4]. Solid squares are MMCDF calculations [30].

to show the amount of the disagreement. The threshold energies assumed for the two sets of calculations are shown. Near threshold the effect of relaxation is to reduce the slope of the photoionization cross section and lower the peak value from 39.1 Mb to 34.0 Mb. At a photon energy of approximately 1 a.u., the RRPAR calculations including relaxation become larger than the unrelaxed RRPA calculations. It is a typical feature of relaxation effects to redistribute the oscillator strength to higher photoelectron energies. This can be thought of in terms of the photoelectron being given an additional boost in kinetic energy due to relaxation of the remaining electrons. The RRPA is expected to be in better agreement with experiment than RRPAR at higher photoelectron energies since relaxation does not have time to take effect when the photoelectron is fast.

For comparison puroposes we have also plotted, in Fig. 1(a), the MBPT calculations of Wijesudera and Kelly [29] and the recent MMCDF calculations of Tulkki [30]. The MBPT calculation does not include relaxation explicitly but does include coupling among various channels including satellite channels and RPAE-type diagrams. The series of resonances preceding the $3s$ threshold in the MBPT calculation result from interactions between $3s\rightarrow np$ excited states and the $3p$ channel. The MMCDF calculation includes relativistic effects, interchannel coupling, relaxation effects, but no RPAE-type diagrams. Clearly the RPAE effects are important for photoionization of the valance subshell.

The RRPAR total photoionization cross section and the partial $3p_{1/2}$ and $3p_{3/2}$ cross sections are shown in Fig. 1(b). The sum of the partial $3p_{1/2}$ and $3p_{3/2}$ cross sections is not identical with the total photoionization cross section in the RRPAR since the partial cross sections are reduced by approximately 4% by the inclusion of overlap integrals among the various spectator electrons.

The branching ratio $\gamma=\sigma(3p_{3/2})/\sigma(3p_{1/2})$, shown in Fig. 1(c), deviates from the statistical ratio of 2 over this energy region. Spin-orbit splitting of the threshold energies along with the overall cross-section shape account for most of the structure seen in the branching ratios. The $3p_{1/2}$ cross section has a shape similar to the $3p_{3/2}$ cross section (scaled down by a factor of 2), but lagging by the spin-orbit splitting of the thresholds, approximately 0.0066 a.u. Thus, when the $3p_{3/2}$ cross section is increasing (decreasing), the branching ratio is greater than (less than) 2.

The angular-distribution asymmetry parameters for the $3p$ subshells are shown in Fig. 1(d) along with the experimental measurements of Houlgate *et al.* [4]. Relaxation effects are minor near threshold. As it is expected for photon energies above approximately 1.5 a.u., the unrelaxed RRPA calculation is in better agreement with experiment than the relaxed calculation. The MMCDF results [30] are also shown and agree fairly well with the RRPAR results.

B. The 3*s* subshell

The penultimate subshell of argon has proven interesting because of strong interchannel coupling between the 3s channels and the predominant $3p$ channels [8]. The Cooper minimum of the $3p$ subshell cross section leads to a corresponding minimum in the $3s$ subshell cross section. In this

study, we have calculated the photoionization parameters using three different models. The RRPA calculations include most effects of both ground- and final-state correlations. Calculations in the RRPAR model include RRPA effects as well as relaxation effects by calculating continuum orbitals in the potential of a relaxed ion and using the experimental thresholds. In the RRPAR, overlap integrals are included between the various spectator electrons of the ionic core when calculating partial cross sections for a specific subshell. The third technique, RRPARA, contains relaxation effects as in the RRPAR, but also accounts for Auger decay of $3p$ electrons into the $3s$ hole state by including energy-dependent rearrangement terms in the dipole matrix element that result from overlap integrals between continuum orbitals and $3p$ ground-state orbitals. In this instance, the specific term added to the RRPAR dipole matrix element is

$$-\frac{(D_{3s\rightarrow 3p_j'})\langle 3p_j|\epsilon p_j'\rangle}{\langle 3p_j|3p_j'\rangle}. \tag{4}$$

Partial photoionization cross sections for the $3s$ subshell obtained by the RRPA, RRPAR, and RRPARA methods are shown in Fig. 2(a) along with the experimentally measured cross sections of Marr and West [2], Houlgate *et al.* [31], Lynch *et al.* [32], and recent measurements by Möbus *et al.* [10]. The effect of the strong interchannel coupling with $3p$ channels ensures that all three models obtain a minimum at approximately the same energy, although the RRPARA calculation never exactly vanishes. Ignoring the shift in threshold, it appears as if relaxation has enhanced the cross section at low photoelectron energies, perhaps by displacing oscillator strength from bound-bound transitions below threshold. Auger decay from the $3p$ subshell has enhanced the cross section for energies below the minimum and decreased the cross section for higher energies. The RRPARA calculations are in excellent agreement with the recent measurements of Möbus *et al.* [10] at energies below 2.0 a.u., although the theory does not reproduce double-electron resonances just above threshold. Partial $3s$ photoionization calculations in MBPT by Wijesundera and Kelly [29] are in better agreement with experiment above 2 a.u. This is probably due to inclusion of coupling with satellite channels that remove flux from the main-line $3s$ cross section. Results from MMCDF calculations [30] are also shown. Although the MMCDF has relaxation included similarly to the RRPARA and interchannel coupling, it does not include all the diagrams that characterize the RPAE. The total photoionization cross sections shown in Fig. 2(b) are due in large part to contributions from the $3p$ subshell and appear relatively insensitive to the effects of Auger decay in this region.

The angular-distribution asymmetry parameter β_{3s} [shown in Fig. 2(c)] is affected strongly by Auger decay. Both the RRPA and RRPAR results show large departures from the nonrelativistic value of 2 at the location of the Cooper minimum. Including Auger effect terms [Eq. (4)] prevents the matrix elements from going completely to zero at the minimum, thus suppressing the reduction in the angular-distribution asymmetry parameter. The RRPARA calculations are in reasonable agreement with the recent measurements of Möbus *et al.* [10]. The MMCDF calculations including relaxation [30] are also in resonable agreement apart from a small energy shift.

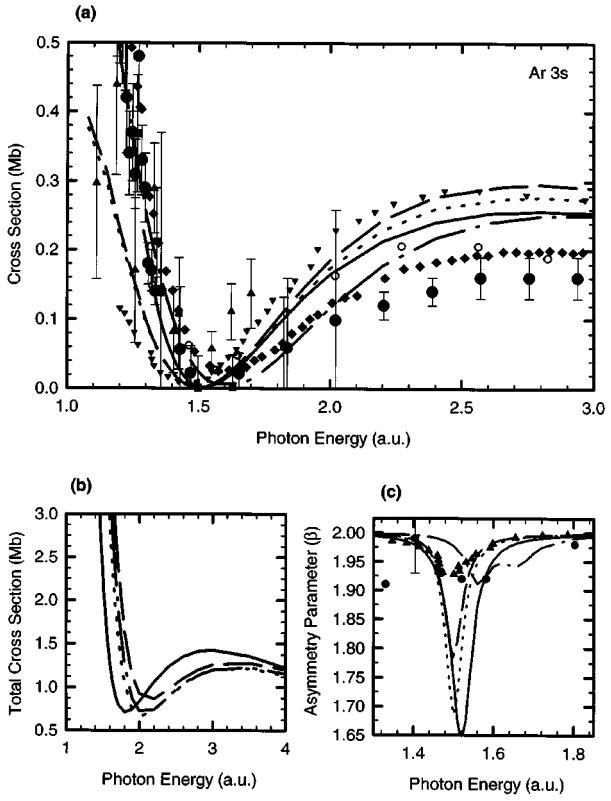

FIG. 2. Theoretical and experimental data for photoionization of the argon $3s$ subshell. (a) The solid line is the RRPA, the dashed (dotted) line is the RRPAR length (velocity) form, and the dot-dashed curve is the geometric mean of the RRPARA. The experimental data are represented by solid dots, Möbus *et al.* [10]; open circles, Marr and West [2]; squares, Houlgate *et al.* [31]; and triangles, Lynch *et al.* [32]. MMCDF calculations [30] are inverted triangles; MBPT [29] are diamonds. (b) Total photoionization cross sections displayed with the same line representation as in (a). (c) Angular-distribution asymmetry parameters. Experimental data (solid dots) are from Möbus *et al.* [10]. MMCDF calculations [30] are triangles.

When relativistic effects are neglected, the angular-distribution asymmetry parameter for photoelectrons originating in an s subshell of a closed-shell atom has the value of 2 independent of energy. The dip seen in Fig. 2(c) is due to coupling between the $3s\rightarrow kp_{3/2}$ channel and the $3s\rightarrow kp_{1/2}$ channel in the vicinity of the minimum of the cross section. Applying the formulation for the electric dipole asymmetry parameter to the present case gives [34]

$$\beta_{3s}=\frac{2D_{3/2}^2+4D_{1/2}D_{3/2}\cos(\delta_{1/2}-\delta_{3/2})}{D_{1/2}^2+2D_{3/2}^2}, \tag{5}$$

where D_j are the dipole matrix elements and δ_j are the phase shifts. When the matrix elements $D_{1/2}$ and $D_{3/2}$ are approximately equal and the phase shifts $\delta_{1/2}$ and $\delta_{3/2}$ are approximately equal, β_{3s} is approximately 2. In the vicinity of the Cooper minima where the two channels may have minima at slightly different energies, the matrix elements may be quite different causing deviations of β_{3s} from 2. Adding contribu-

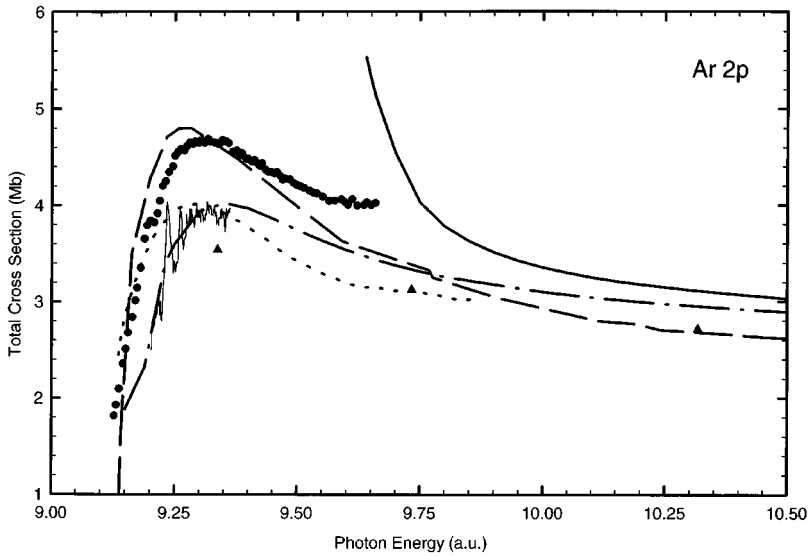

FIG. 3. Total photoionization cross sections for the argon $2p$ subshell. Theory: thick solid line, the unrelaxed RRPA total cross section; dot-dashed line, the RRPARA that includes relaxation effects; dotted line, the GRPAE by Amusia [21]; and dashed line, MBPT including polarization by Pan and Kelly [33]. Experiment: solid dots, Deslattes [12]; solid triangles, Lukirskii and Zimkina [11]; and thin solid line, Nakamura *et al.* [13]. The data from Nakamura *et al.* was not on an absolute scale and was scaled for this figure to the RRPARA calculation at 9.30 a.u.

tions from Auger decay to the dipole matrix elements prevents the matrix elements from vanishing and thus smooths the dip in β_{3s}.

C. The $2p$ subshell

The importance of rearrangement in calculations of the $2p$ subshell cross section of Ar is clear in Fig. 3. The total photoionization cross-section results in the RRPA and RRPARA are plotted along with the nonrelativistic GRPAE calculation of Amusia and Cherepkov [6] and the MBPT calculation including relaxation and polarization effects of Pan and Kelly [33]. The MBPT calculation demonstrates the large effect of polarization diagrams and is approximately in agreement with experiment [12] near the peak; however, they disagree at higher energies. The experimental data shown are from Lukirskii and Zimkina [11], Deslattes [12], and Nakamura *et al.* [13]. The measurements of Nakamura *et al.* [13] have been scaled to agree with the RRPARA at 9.23 a.u. A simple scaling of the measurements of Deslattes [12] would bring them into excellent agreement with the RRPARA calculations. It should be noted that the Auger effects are small and we have not plotted the RRPAR calculations since they are indistinguishable from the RRPARA.

In Fig. 4(a) we show the breakdown of the total photoionization cross section into various partial cross sections above the $2p$ photoionization threshold in the RRPARA. The total photoionization cross section is shown without the reduction due to overlap integrals among the spectator electrons; this then includes, approximately, the contributions of double-photoionization and photoionization-with-excitation channels in the total. The $2p_{3/2}$ and $2p_{1/2}$ partial cross sections are also shown, as is the sum of all $3s$ and $3p$ channels.

Figure 4(b) is a comparison between the partial $2p$ photoionization cross section calculated in the RRPA and RRPARA. An overall reduction in the RRPARA cross section is due to overlap integrals of the sudden approximation redistrubuting flux to multiple-excitation channels. The large, energy-dependent change in the cross section is due to differences in the potential of the outgoing photoelectron. Corresponding differences are noted in the branching ratio $\gamma=\sigma(2p_{3/2})/\sigma(2p_{1/2})$ plotted in Fig. 4(c). The relaxed cross sections that begin with positive slope lead to $\gamma>2$, whereas the RRPA cross sections beginning with negative slope lead to $\gamma<2$.

Angular-distribution asymmetry parameters for the RRPA and RRPARA are shown in Fig. 4(d) along with the data of Lindle *et al.* [14], taken at two different synchrotron sources, and Avaldi *et al.* [15]. It is possible that the discrepancy between theory and experiment near 9.5 a.u. is due to polarization effects, which Pan and Kelly [33] demonstrated are significant in $2p$ cross-section calculations.

D. The $2s$ subshell

The effects of interchannel coupling and rearrangement on the $2s$ subshell cross section of Ar were studied by Lavrentev *et al.* [17] in the framework of the nonrelativistic RPAE and included rearrangement with a technique similiar to that used in the present RRPARA model. Experimental measurements of the $2s$ partial cross sections were reported by Lukirskii and Zimkina [16].

Results of the RRPA, RRPAR, and RRPARA calculations are plotted in Fig. 5 along with the experimental measurements [17] and the RPAE calculations of Lavrentev *et al.* [17]. Both the $2p$ and $3p$ subshell electrons can make Auger transitions into the $2s$ hole with $3p\rightarrow 2s$ transitions having the largest effect (70% increase) on the cross section and $2p\rightarrow 2s$ transitions having a smaller effect (6% decrease). Uncertainty in the experimental results hinders an accurate

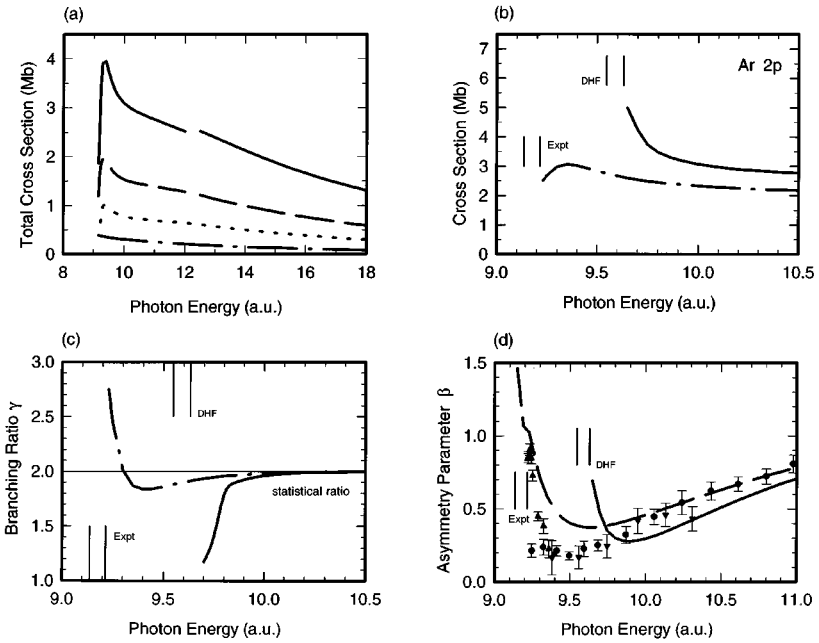

FIG. 4. Photoionization parameters for the argon $2p$ subshell. (a) Solid line, total photoionization cross section; dashed line, partial $2p_{3/2}$ cross section; dotted line, partial $2p_{1/3}$ cross section; and dot-dashed line, sum of other single-excitation channels in the RRPARA. (b)–(d) Solid line, the RRPA; dot-dashed line, the RRPARA geometric mean. The RRPAR and RRPARA are indistinguishable. The branching ratio γ in (c) is defined by $\gamma=\sigma(2p_{3/2})/\sigma(2p_{1/2})$. The experimental data are shown in (d) by solid dots and inverted triangles, Lindle *et al.* [14], and triangles, Avaldi *et al.* [15].

comparison between the various theoretical predictions and experiment. It is hoped that the present work will stimulate further experimental work on this subshell cross section. The excellent agreement between the RRPARA and RPAE [17] calculations shows that relativistic effects are minimal in the case.

E. The 1*s* subshell

Deep inner-shell photoionization is influenced by a number of effects. Rearrangement, radiative decay, Auger decay, and post-collision interaction can all play a role. The importance of the effects of rearrangement and Auger decay can be

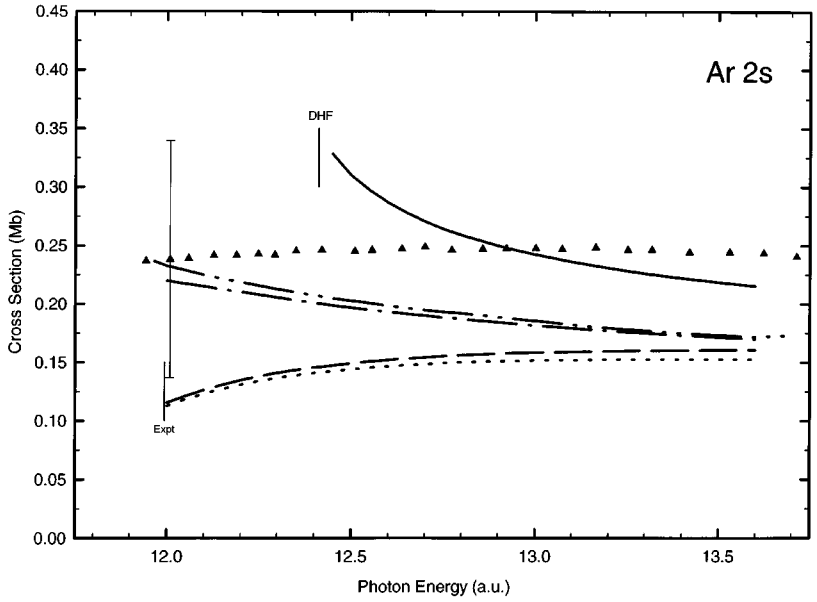

FIG. 5. Partial photoionization cross sections for the $2s$ subshell of argon. The solid line is RRPA; the dashed (dotted) line is the RRPAR length (velocity) form. The dot-dashed line is the geometric mean of length and velocity for the RRPARA. The RPAE including relaxation [17] is given by the double-dot–dashed line. The experiment, represented by solid triangles, is from Lavrentev *et al.* [17]. A representative error bar is shown for the experiment.

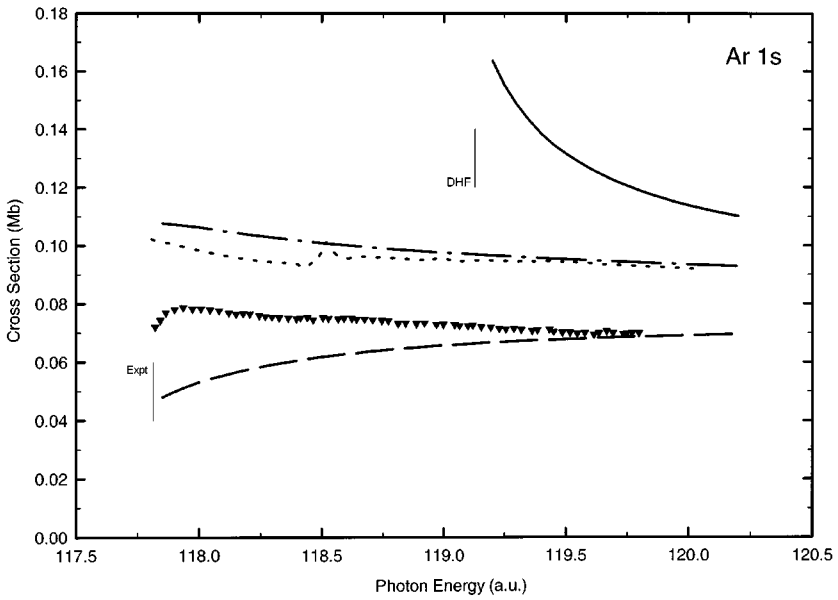

FIG. 6. Photoionization cross sections of the $1s$ subshell of argon. The solid line is the RRPA and the dashed (dot-dashed) line is the geometric mean of the RRPAR (RRPARA) length and velocity forms. The inverted triangles are calculations allowing for $1s$ vacancy Auger decay by Amusia [21]. The dotted line is from the experiment of Deslattes *et al.* [18].

seen in Fig. 6, where the total photoionization cross sections in the RRPA, the RRPAR, and the RRPARA are shown along with the RPAE calculation of Amusia and Cherepkov [6] including $1s$ vacancy Auger decay and the experimental absolute measurement of Deslattes *et al.* [18]. The RRPA result (which includes no rearrangement effects) has clearly the wrong distribution of oscillator strength near threshold, but eventually converges to the measured values. The effect of relaxation (as in the RRPAR result) is to drastically reduce the cross section near threshold. The inclusion of relaxation and Auger decay (RRPARA) leads to improved agreement between theory and experiment. The RRPARA calculation cross section is somewhat large near threshold and also does not account for the resonance structure seen at 0.70 a.u. above threshold. Saha [22] has determined that this is a double-electron resonance where $1s$ and $3p$ electrons are virtually excited into a $3d^2$ state.

As is the case with the $2s$ subshell, both the $2p$ and $3p$ subshell electrons can make Auger transitions into the 1s hole with $3p \rightarrow 1s$ transitions having the largest effect on the cross section (77% increase) and $2p \rightarrow 1s$ transitions having a smaller effect (30% increase).

Significant differences are to be noted between the $1s$ Auger decay calculation of Amusia and Cherepkov [6] and the present result. Two physical effects could possibly account for the difference: (a) Relativistic effects are included in the RRPARA calculation but not in the RPAE calculations and (b) Amusia and Cherepkov [6] include $1s$ vacancy Auger decay by calculating the wave function of the slow photoelectron in the field of the doubly ionized rather than of the singly ionized residual ion. This second effect is almost certainly more important than relativistic effects since spin-orbit splitting of thresholds is not a large factor here.

IV. CONCLUSION

Photoionization cross sections, branching ratios, and photoelectron angular-distribution asymmetry parameters have been calculated in the RRPA, RRPAR, and RRPARA models for all subshells of argon. Relaxation effects are seen to increase as deeper inner-subshells are considered. The $1s$, $2s$, and $2p$ subshell cross sections are all very sensitive to relaxation. Auger decay was found to be an important contribution to the cross section for $1s$ and $2s$ subshells, but not for the $2p$ subshell.

None of the calculations explicitly included the effects of core polarization. These polarization effects should be included in photoionization calculations near the $2p$ and $3p$ thresholds since the s wave potential, having no centifugal term, may change considerably when a short-range polarization potential is added.

This study has highlighted the need for more accurate experimental measurements for the deep inner shells of argon, especially the $2s$ subshell. The new generation of synchrotron sources should make such measurements possible.

ACKNOWLEDGMENTS

This work was partially supported by a grant from the Andrews University Office of Scholarly Research. The authors wish to thank V. Radojević for use of the RRPAR code and Walter Johnson for use of the RRPA code.

[1] J. A. R. Samson, Adv. At. Mol. Phys. **2**, 177 (1966).
[2] G. V. Marr and J. B. West, At. Data Nucl. Data Tables **18**, 497 (1976).
[3] T. N. Chang, Phys. Rev. A **15**, 2392 (1977).
[4] R. G. Houlgate, J. B. West, K. Codling, and G. V. Marr, J. Electron Spectrosc. **9**, 205 (1976).
[5] H. P. Kelly and R. L. Simons, Phys. Rev. Lett. **30**, 529 (1973).
[6] M. Ya. Amusia and N. A. Cherepkov, Case Stud. At. Phys. **5**, 47 (1975).
[7] W. R. Johnson and K. T. Chang, Phys. Rev. **20**, 978 (1979).
[8] M. Ya. Amusia, V. K. Ivanov, N. A. Cherepkov, and L. V. Chernysheva, Phys. Lett. **40A**, 361 (1972).
[9] H. Kossmann, B. Krassig, V. Schmidt, and J. E. Hansen, Phys. Rev. Lett. **58**, 1620 (1987).
[10] B. Möbus, B. Magel, K.-H. Schartner, B. Langer, U. Becker, M. Wildberger, and H. Schmoranzer, Phys. Rev. A **47**, 3888 (1993).
[11] A. P. Lukirskii and T. M. Zimkina, Bull. Acad. Sci. USSR Phys. Ser. **27**, 808 (1963).
[12] Richard D. Deslattes, Phys. Rev. **186**, 1 (1969).
[13] M. Nakamura, M. Sasanuma, S. Sato, M. Watanabe, H. Yamashita, Y. Iguchi, A. Ejiri, S. Nakai, S. Yamaguchi, T. Sagawa, Y. Nakai, and T. Oshio, Phys. Rev. Lett. **21**, 1303 (1968).
[14] D. W. Lindle, L. J. Medhurst, T. A. Ferrett, P. A. Heimann, M. N. Piancastelli, S. H. Liu, D. A. Shirley, T. A. Carlson, P. C. Deshmukh, G. Nasreen, and S. T. Manson, Phys. Rev. A **38**, 2371 (1988).
[15] L. Avaldi, G. Dawber, R. Camilloni, G. C. King, M. Roper, M. R. F. Siggel, G. Stefani, and M. Zitnik, J. Phys. B **27**, 3953 (1994).
[16] A. P. Lukirskii and T. M. Zimkina, Bull. Acad. Sci. USSR, Phys Ser. **27**, 817 (1963).
[17] S. V. Lavrentev, V. L. Sukhorukov, A. N. Khoperskii, and I. D. Petrov, Opt. Spectrosc. (USSR) **62**, 466 (1987).
[18] R. D. Deslattes, R. E. Lavilla, P. L. Cowan, and H. Henins, Phys. Rev. A **27**, 923 (1983).
[19] J. Tulkki and T. Åberg, J. Phys. B **18**, L489 (1985).
[20] J. W. Cooper, Phys. Rev. A **38**, 3417 (1988).
[21] M. Ya. Amusia, in *Atomic Photoeffect*, edited by P. G. Burke and H. Kleinpoppen (Plenum, New York, 1990), p. 201.
[22] H. P. Saha, Phys. Rev. A **42**, 6507 (1990).
[23] W. R. Johnson and C. D. Lin, Phys. Rev. **20**, 964 (1979).
[24] V. Radojević, M. Kutzner, and H. P. Kelly, Phys. Rev. A **40**, 727 (1989).
[25] T. Åberg, in *Photoionization and Other Probes of Many-Electron Interactions* (Plenum, New York, 1976).
[26] T. Åberg, in *Inner-Shell and X-Ray Physics of Atoms and Solids*, edited by D. J. Fabian, H. Kleinpoppen, and L. M. Watson (Plenum, New York, 1981).
[27] I. P. Grant, B. J. McKenzie, P. H. Norrington, D. F. Mayers, and N. C. Pyper, Comput. Phys. Commun. **21**, 207 (1980).
[28] H. Siegbahn and L. Karlsson, in *Corpuscles and Radiation in Matter*, edited by W. Mehlhorn, Handbuch der Physik Vol. 31 (Springer-Verlag, Berlin, 1982), p. 317.
[29] W. Wijesundera and H. P. Kelly, Phys. Rev. A **39**, 634 (1989).
[30] J. Tulkki, Phys. Rev. A **48**, 2048 (1993).
[31] R. G. Houlgate, J. B. West, K. Codling, and G. V. Marr, J. Phys. B **7**, L470 (1974).
[32] M. J. Lynch, A. B. Gardner, K. Codling, and G. V. Marr, Phys. Rev. Lett. **43A**, 237 (1973).
[33] Cheng Pan and H. P. Kelly, Phys. Rev. A **39**, 6232 (1989).
[34] S. T. Manson and A. F. Starace, Rev. Mod. Phys. **54**, 389 (1982).